PULSE-INDUCED CRITICAL SCATTERING (PICS) FROM POLYMER SOLUTIONS

KENNETH W. DERHAM, JOHN GOLDSBROUGH and MANFRED GORDON

Institute of Polymer Science and Department of Chemistry
University of Essex, Wivenhoe Park, Colchester, CO4 3SQ, UK

ABSTRACT

Pulse-induced critical scattering (PICS) is a new, fast technique for determining thermodynamic and kinetic parameters of polymer solutions. Relative intensities of scattered laser light are measured over periods of seconds after a fast temperature step into the region of Debye critical opalescence. In the mode of operation using thermal pulses to progressively lower temperatures, the intensity pulse shape gives sensitive information on the fluctuation equilibrium and on the kinetics of phase separation with formation of emulsions of sub-wavelength particles. Spinodal and critical loci for the system polystyrene–cyclohexane (PS–CH) are measured about 10 times faster and more accurately than in recent work based respectively on conventional light scattering equipment and on turbidimetry. The classical Debye theory of scattering near a critical point, or Scholte's extension to spinodal points, gives excellent semi-empirical extrapolations to spinodal temperatures T_s. Though there are signs that the classical theory needs amendment in the sense of the generalized non-linear theory of Fisher, Chu, and co-workers, this would generally give results on T_s in close agreement with the simpler classical theory in the experimental range accessible to PICS. The effects of heterodispersity on the phase diagram are studied, comparing data by Scholte and new data by PICS on PS–CH. The evidence suggests that spinodal loci are governed mostly by M_w (as suggested by recent theories). Marked secondary effects seem, however, to arise, not (as recently suggested) from M_n, but from M_z. Results obtained by the technique of approaching phase equilibrium from the heterogeneous side, using an emulsion carefully 'seeded' by a thermal step, suggest that supercooling is more serious in cloud-point determinations of *dilute* polymer solutions than hitherto thought. The formation of sub-wavelength droplets follows kinetics bearing more than formal resemblance to that for the nucleation and growth of spherulitic crystals in bulk.

1 INTRODUCTION

Useful structural and thermodynamic information on polymers can be derived from semi-empirical fits of measurements on phase equilibria of solutions, a subject much advanced by Koningsveld[1] and his co-workers. Recent progress in technology, especially the advent of the laser, has wrought much improvement in the relevant measurement techniques. Pulse-Induced

Critical Scattering (PICS) was developed as a result of these stimuli. Evidence is presented that such an instrument measures spinodal and cloud points of polymer solutions faster than, but at least as accurately as, the best equipment has achieved hitherto. The reliability of the quantitive interpretation of scattering intensities is increased by correlating thermodynamic and kinetic quantities. In Section 2, we recall the typical phenomenology and underlying molecular causes of polymer solutions near a Θ-point. The rationale of applying rapid thermal steps, and examining the effect on light scattering over a time-scale of seconds, is firmly rooted in the basic molecular events, according to the theory of critical scattering by Debye and co-workers[2–4], recently improved by Vrij and van den Esker[5]. Scholte[6] extended this classical theory to the determination of spinodals of polymer solutions, and Chu, Schoenes and Fisher[7]—and later Chu and co-workers[8]—made more accurate measurements and used a generalized non-linear theory to fit them. For the purposes of this work, the classical linear theory is found to be adequate.

2 THE TYPICAL PHASE DIAGRAM

A schematic phase diagram of temperature T vs. concentration (volume fraction ϕ) of polymer is shown in *Figure 1* for a polymer solution just below its Flory Θ-point, e.g. polystyrene (PS)–cyclohexane (CH). As is familiar, such a diagram is merely rotated through 180° about a line parallel to the

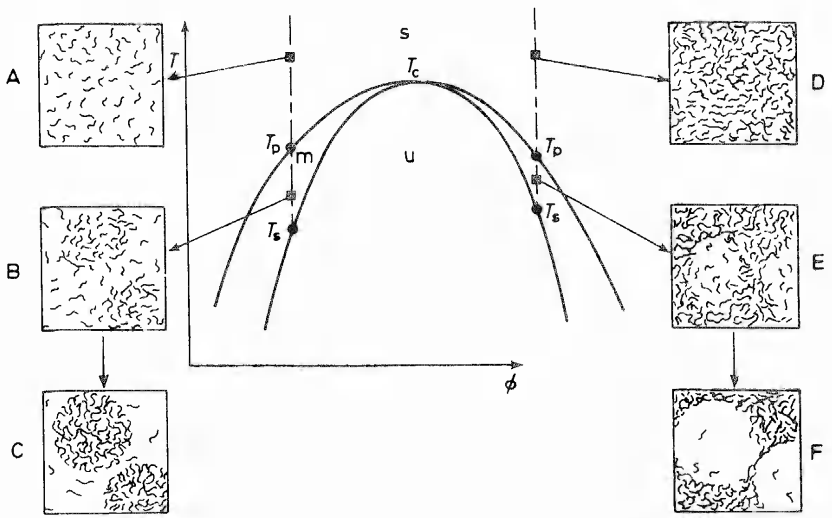

Figure 1. Schematic phase diagram of temperature vs. concentration. s–stable, m–metastable, and u–unstable solutions. T_p points on cloud-point curve, T_s on spinodal curve, T_c critical point. Dilute solutions: A–stable, B–metastable fluctuation equilibrium at short times, C–separate phases (emulsion) at longer times. Concentrated solutions: D–stable, E–metastable fluctuation equilibrium at short times, F–separate phases (emulsion) at longer times

concentration axis, when applied to the region of a Rowlinson Θ-point. In such cases, e.g. polyethylene–octane, upper critical solution temperatures are replaced by lower ones, and PICS requires heating pulses instead of cooling ones (see below), but nothing is changed in principle as far as the present work is concerned.

Figure 1 shows the three temperature–concentration regions which generally occur in a quasi-binary phase diagram. Stable solutions at high temperatures are separated from metastable solutions at lower temperatures by the binodal or cloud-point curve; the metastable region is in turn separated from that of unstable solutions at even lower temperatures by the so-called spinodal. The spinodal is immensely important in technology, e.g. of metals and ceramics, as well as in polymer science, because of the 'spinodal decomposition' which can occur there—for a recent review see Goldsbrough[9]. Thermodynamics requires that the cloud point curve and the spinodal share a common tangent at the critical point (ϕ_c, T_c). For a truly binary (homodisperse) solution, T_c occurs at the maximum temperature of the binodal; for heterodisperse polymers it occurs to the right of the maximum (Chermin *et al.*[10]).

The molecular events are schematized in the figure, both for solutions more dilute (A, B, C), and more concentrated (D, E, F) than ϕ_c. At short times of residence in the metastable region between cloud point and spinodal, fluctuation regions are seen, which normally reach a metastable fluctuation equilibrium (cf. Section 5). The closer the temperature to the spinodal, the less time is available to study this metastable state. Soon a local fluctuation of high (B) or low (E) concentration ϕ will chance to exceed the critical size for nucleation of a droplet, and such droplets rapidly grow to macroscopic dimensions and develop sharp phase boundaries (C, F). Thus phase separation has occurred. The concentration of the droplet phase separating at $\phi < \phi_c$ is high (C); at $\phi > \phi_c$ it is low (F).

Light scattering permits the study of inhomogeneities in refractive index, whether occasioned by diffuse fluctuation regions (B, E) or by droplets circumscribed by sharp phase boundaries (C, F). To observe scattering from metastable fluctuation regions, we must work rapidly, because metastable solutions below the cloud point curve have lifetimes which progressively shorten as the spinodal is approached. The requisite apparatus is described in Section 3.1.

3 INSTRUMENTATION AND MATERIALS

3.1. The PICS instrument

The instrument for creating thermal pulses and collecting scattering intensity and temperature data has been developed over a number of years. *Figure 2* shows a simple version with a single scattering cell. A more sophisticated multi-cell instrument has recently been built. The thin-walled capillary cell of diameter 1 mm holds a few microlitres of solution. The light source is a low-power He–Ne laser beam passing axially along the cell. Light scattered from the cell is collected by two light guides, one (I_{30}) sampling over scattering angles centred at $\theta = 30°$, the other (I_{90}) at 90°. The light-guides pass the light to a solid-state detector, while temperatures are measured

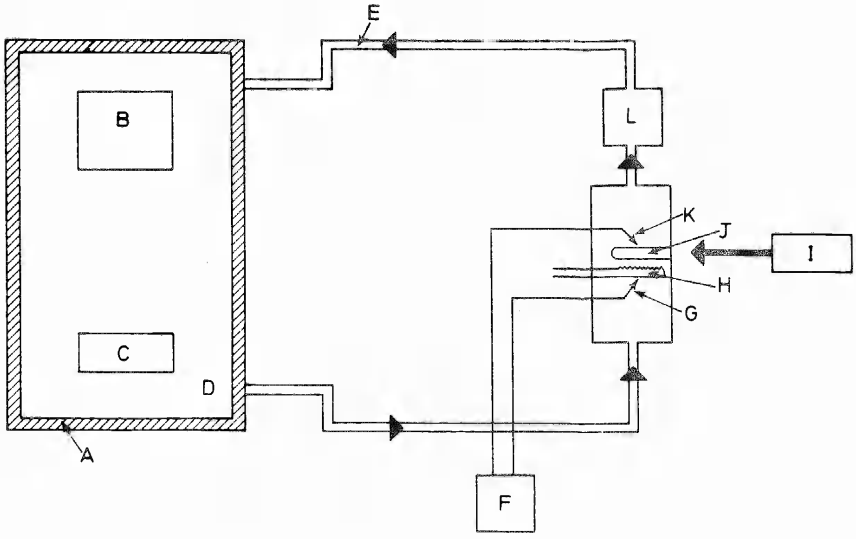

Figure 2. Simplified diagram of PICS apparatus. A–bath, B–immersion heater, C–refrigeration unit, D–heat transfer fluid, E–flow system, F–data handling system, G–light guide, H–heater, I–helium–neon laser, J–scattering cell, K–thermistor, L–pump

by a thermistor. A purpose-built data collection system, based on a Solartron Data Transfer Unit, copes with the high speed of accumulation of measurements. A purpose-built sequence-control unit arranges for the collection of intensity data at the base-line, and at the end of a pulse, later processed by computer. The intensities I_{30} and I_{90} are also displayed in real time on a recorder chart. A typical pattern for measurements in the stable region just above the cloud point is shown in *Figure 3*.

The cell is placed in a water flow system with a small heater situated upstream from the cell to maintain it at a temperature above the cloud point. The temperature step is produced by switching off the heater. The cell contents then cool down rapidly to the temperature of the flowing water. With the most up-to-date method of producing cooling pulses, the thermal response time is about 1 s, as checked by placing a bead thermistor inside the cell. This agrees with the typical delay of about 5 s (*Figure 3*) before maximum fluctuation scatter is attained at the beginning of a pulse ($e^{-5} \approx 0.007$). Fluctuation scattering equilibrium, either stable above the cloud point or metastable below the cloud point, is always attained in less than 5 s. It is not, therefore, at present possible to study relaxation from state A to state B, say, in *Figure 1* after a thermal step. The kinetics of phase change, from state B to C, however, is readily followed by the pulse technique (see Section 6.2). Temperature calibration of the thermistor is against a platinum resistance thermometer calibrated by the National Physical Laboratory. Maximum drift over a 14 months period was 0.02°C over the range 20 to 40°C, and the small corrections resulting from drift were applied.

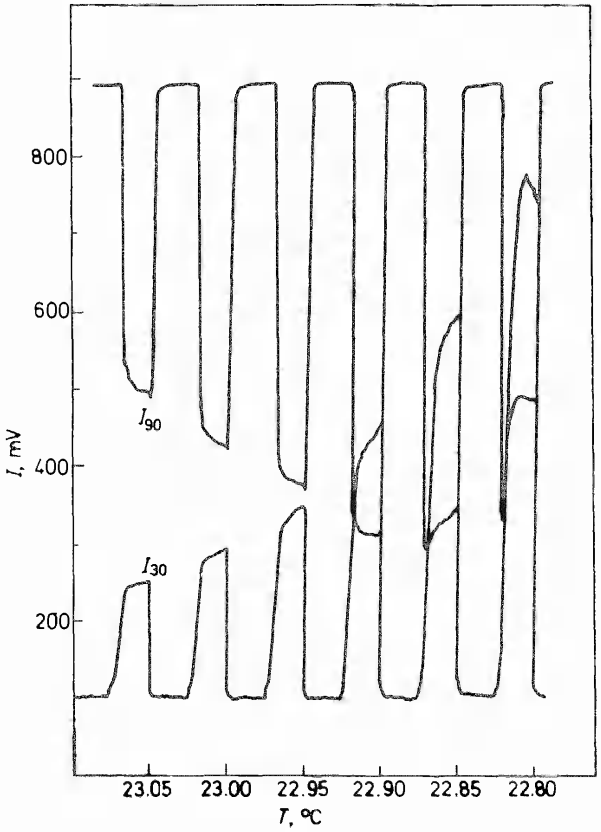

Figure 3. Typical PICS light scattering intensity vs. temperature diagram during cooling run at high concentration (0.15 w/w PS200). Top: intensity at 90° (scale increasing downward). Bottom: intensity at 30° (scale increasing upward). The millivolt output scales for I_{30} and I_{90} are not directly comparable, as I_{90} is amplified more strongly

3.2 Materials

Cyclohexane (CH) was the British Drug Houses spectroscopic grade, dried over molecular sieve. The polystyrene samples were sharp fractions purchased from Pressure Chemicals, with the maker's specifications given in *Table 1*. The fractions were coded PS527 for the sample of $\bar{M}_w = 5.27 \times 10^5$ etc., see *Table 1*. Mixtures of these fractions were made up and their molecular weight averages calculated as shown in *Table 1*. All solutions were kept in sealed ampoules for more than 24 hours at *ca.* 50°C with occasional shaking before filling and sealing the capillary cells. These cells themselves were stored at 50°C when not in use.

Table 1. Samples of polystyrene studied in this work and by Scholte[11]

Sample	Composition	Mol. weights × 10^{-3} M_n	M_w	M_z	M_w/M_n	Ratios M_z/M_w
Narrow fractions						
PS 33	—	36	33	—	~1	—
PS 51	—	49	51	55	1.04	1.08
PS 111	—	111	111	—	~1	—
PS 166	—	154	166	181	1.08	1.09
PS 200	—	193	200	—	1.04	—
PS 527	—	490	527	593	1.08	1.12
Bimodal mixtures						
1 (Scholte[11])	—	70	100	131	1.43	1.31
2 (Scholte[11])	—	38	100	150	2.63	1.50
3 (Scholte[11])	—	22	100	157	4.62	1.57
PSM 6	0.534 g PS33 + 0.466 g PS200	54	110	173	2.05	1.56
PSM 5	0.716 g PS33 + 0.284 g PS527	45	165	432	3.68	2.62

4 LOCATION OF CRITICAL POINTS (DEBYE ET AL.)[2–4] AND SPINODAL POINTS (SCHOLTE)[6]

The precise nature of the mathematical singularity at critical points is not settled. However, the sensitive way in which the scattering intensity varies beyond the immediate neighbourhood of the singularity may be taken from the classical theory of Debye *et al.*[2–4] who derived a formula of the following form, which is practically linear in $1/(T - T_c)$ over the small ranges of T concerned:

$$I = TP(\theta)/[a(T - T_c) + b\sin^2(\theta/2)] \tag{1}$$

Here $P(\theta)$ is the particle scattering factor and a and b are constants. According to this equation, the intensity would appear to diverge at $T = T_c$ in the direction of the beam ($\theta = 0$), while at finite angle θ this catastrophe would be averted by the term $b\sin^2(\theta/2)$ in the denominator. A plot of $1/I$ vs. T would remain almost linear until $b\sin^2(\theta/2)$ became comparable with $a(T - T_c)$. For $\theta = 30°$, this is calculated to occur at $T - T_c < 0.03°C$ within the range of molecular weights of PS in CH here studied. The calculation is based on the revised characteristic lengths l given by Vrij and Van den Esker[5], e.g. *ca.* 3 nm at $M = 5 \times 10^5$. Linear plots, unaffected by the angle-dependent term $b\sin^2(\theta/2)$, are therefore predicted up to very close to the critical point. Scholte propounded the corresponding theory for spinodal points, and he found experimentally plots of ΔI^{-1} vs T^{-1} to be linear for PS–CH. Here ΔI is the difference in scattering intensity between solution and solvent. Deducting the small solvent scattering effect is equivalent to eliminating the small amount of scatter attributable to density fluctuations, which are superposed on the concentration fluctuations of interest. Scholte's results, obtained with standard light-scattering equipment, are here broadly

confirmed and extended by PICS to a wider range of PS samples, with an increase in accuracy from a few tenths to a few hundredths of a degree. We have eliminated the extrapolation to $\theta = 0°$ scattering angle because the angle effect on the apparent spinodal temperature is certainly small at $\theta = 30°$, and would at worst produce a very small parallel shift of the spinodal locus in a phase diagram. We comment on the work of Chu *et al.*[8] in the Discussion (Section 7).

5 MEASUREMENTS OF SPINODAL POINTS BY PICS

The rationale of locating a spinodal point by PICS rests on extrapolation of the Scholte plot of Δl^{-1} to T_s^{-1} on the T-axis. As we are concerned with plots ranging over <2 degrees at ~ 300 K, we simplify throughout by plotting $(\Delta l)^{-1}$ against T rather than T^{-1}. A large number of experimental points at temperature intervals of 0.01 degree or less are collected by a

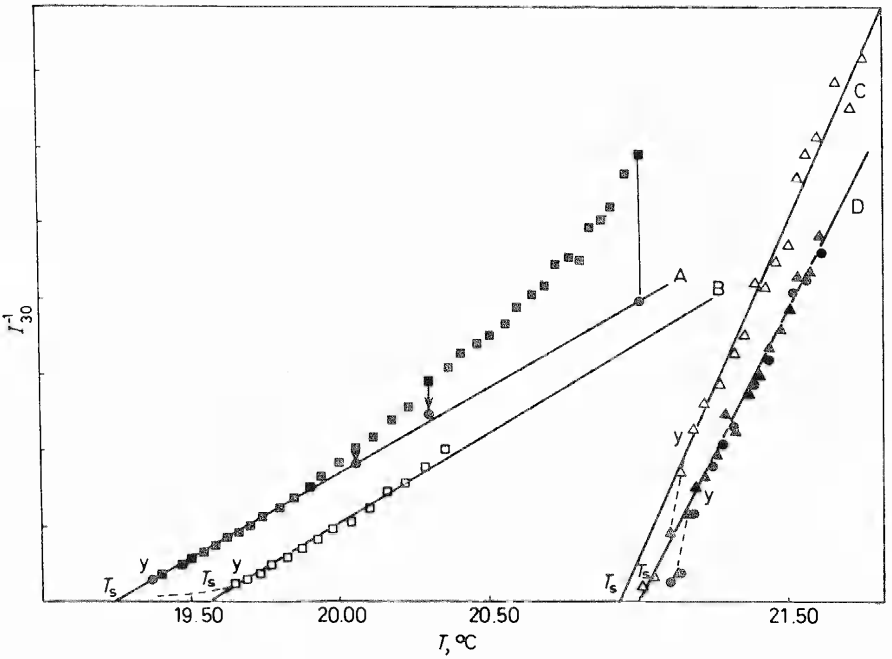

Figure 4. Typical extrapolation procedure to locate spinodal points T_s. A–0.155 w/w PSM 6; B–0.140 w/w PSM 6; C–0.154 w/w PS 111; D–0.144 w/w PS 111. Plot A illustrates the empirical linearization by the parameter c for four selected points ■ → ●; the point nearest T_s is not visibly shifted by this correction. In plot B, points at high temperature omitted for clarity. In plot D, ● and ▲ refer to replicate runs. y marks the last acceptable pulse in each run before phase change invalidates the pulse profile (see *Figure 3*). According to the second-approximation theory (Section 7.3), plots A and C should have the same T_s, and the same would apply to B and D, since each pair share almost exactly the same ϕ and M_w

controlled cooling rate of the circulating water, e.g. at 0.1 deg min^{-1}. An average of four intensity measurements at the end of a 20 s cooling pulse gives a measure of I_{30} of the solution. The value of I_{30}^0 for the solvent can be obtained approximately from the same solution at sufficiently high temperature to suppress fluctuation scattering, or by placing a similar cell containing cyclohexane in the beam. In practice, we prefer to make an empirical correction to such an estimate of I_{30}^0, typically of order 10–30% of the lowest intensity pulse included in an extrapolation plot, and <4% of the most intense pulse. The magnitude of the correction c is determined by linearizing the plot of $(I_{30} - c)^{-1}$ vs T. It has little effect (*Figure 4*) on the extrapolated value of T_s. Interference by incipient phase change with the recorded pulse-height intensities at the high-intensity end of the plot would have the most serious effect on the extrapolation to T_s. Such interference generally leads to artificially raised I_{30} at low concentration ϕ, and artificially low I_{30} at high ϕ. Fortunately, in both cases, the onset of the trouble is sharp, and well signalized by changes in the profile of the intensity pulses. In *dilute solutions*, the separation of even a small amount of droplets of a concentrated solution phase always causes a sudden marked rise in I_{30}, above the low level due to fluctuation scattering. This is shown in *Figure 5*. For a time the fluctuation scattering is still seen as a shoulder on the rising peaks due to scattering from the emulsion, but further cooling rapidly

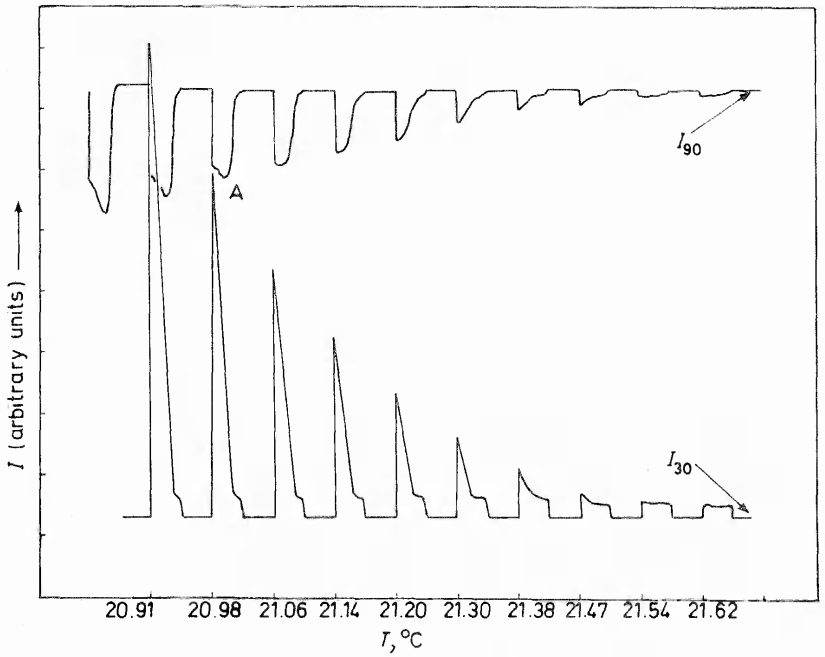

Figure 5. Typical PICS cooling run on dilute solution (0.0100 w/w PS 166). Note low intensity fluctuation-scattering pulses at high temperature, progressively superseded by emulsion scattering spike on I_{30} at lower temperatures. Decline in pulse intensity profile on I_{90} after A is due to the droplet diameter of the emulsion approaching the wavelength (~ 600 nm)

accelerates the phase separation process, so that the shoulder becomes obliterated. In *concentrated solutions*, on the other hand, where critical (fluctuation) scattering is generally stronger, and the separating droplet phase much more dilute, the scattering intensity I_{90} will drop sharply as a result of phase separation. This is illustrated in *Figure 3*. The drop in intensity is attributed to the decrease in critical scattering of the continuous phase, as its spinodal temperature will decrease as a result of the change in composition. The clear and intelligible change in pulse shape allows the limit of approach to T_s to be determined accurately, to which the critical scattering pulses are valid.

Figure 4 is important in providing evidence for effects due to polydispersity. This is taken up in the Discussion (Section 7.3). The extrapolations may be claimed to be reliable to about 0.02 degree K, which is about the standard deviation of replicate runs on the same cell. As noted by Scholte, the determination of T_s becomes progressively less accurate in more dilute solutions.

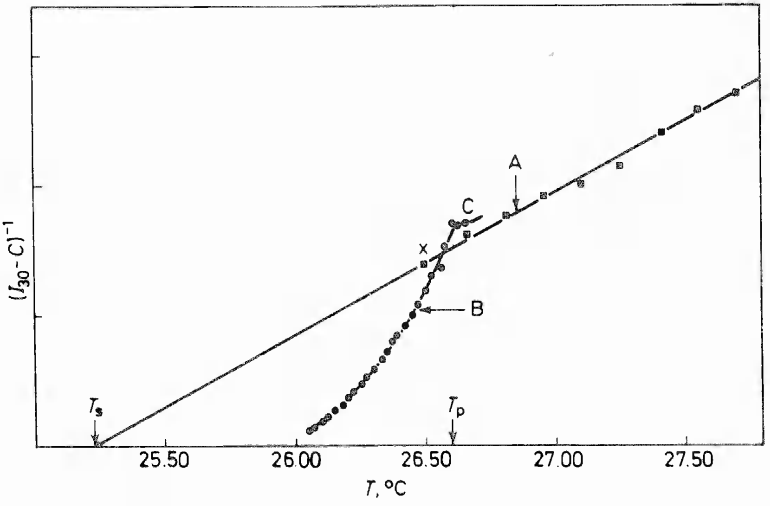

Figure 6. Combined plot of $(I_{30} - c)^{-1}$ vs. T for a relatively dilute solution 0.029 w/w PS527. A pulsed cooling run, B–continuous heating of emulsion. A and B meet at cloud pount T_p. At C, slight displacement of points belonging to stable solution from line A due to experimental error (base line shift)

The accessible critical scattering range is then separated from T_s by a widening gap in which fast phase separation masks the fluctuation scatter. It is known that the cloud point curve rises further above the spinodal curve (cf. *Figure 1*) in dilute polymer solutions, the greater the polydispersity of the polymer. Accordingly, the accuracy of T_s determinations for dilute polydisperse samples is even less than for sharp fractions. We have not succeeded in making measurements of T_s for the mixtures of sharp fractions listed in *Table 1* at $\phi < 0.06$ w/w with our present light detection system.

Figure 6 illustrates the case of a longer extrapolation in a relatively more dilute solution, when phase separation is seen to interfere with the validity of the critical scattering pulses approximately 1.3 degrees above the spinodal. Here the accuracy of T_s is estimated to be ± 0.2 degree C.

6 CLOUD POINT DETERMINATION BY THE PICS INSTRUMENT

Thermodynamic binodal or cloud points can be determined rapidly, and practically without trouble from hysteresis, by approaching the equilibrium from the two-phase side, i.e. by heating PS–CH emulsions. The PICS equipment affords the necessary control over the thermal programming, and the location of the cloud point is deduced from scattering measurements. It is useful to 'seed' the emulsion by a sudden step from above to just below the cloud point, e.g. 0.1°C below the cloud point T_p in concentrated solutions, or 1°C below T_p in dilute solutions. Circumstantial evidence from the scattering behaviour suggests that such emulsions are stable during the short period required for determining the cloud point. We shall illustrate the best procedure for relatively concentrated solutions using as example 0.0843 w/w of PS 111 in CH, and the best procedure for relatively dilute solutions using 0.0144 w/w of PS 111 in CH.

6.1 Concentrated solutions

In concentrated solutions, the problem of cleanly separating the emulsion scattering from the substantial intensity of residual fluctuation scattering, is best achieved using intensity measurements at $\theta = 90°$. As shown in *Figure 3*, I_{90} declines suddenly during a pulse in which the formation of emulsion intervenes. The temperature T_e, say, at which this decline occurs for the time during the PICS run for measuring T_s, is generally suitable for forming the emulsion with which to measure T_p. The cell is suddenly cooled from well above T_p to T_e, and held there until the intensity has decayed to about $\frac{1}{4}$ or $\frac{1}{3}$ of its maximum value, typically in 20 s. The linear heating rate (~ 0.2°C/min) is then switched on. As shown by the points in *Figure 7*, the intensity then rapidly increases with temperature (and time) until the original critical scattering intensity is recovered, which happens at or very near to the sharp maximum in the scattering intensity when plotted against temperature. The position of the maximum is reproducible to 0.02°C or better and is taken as the cloud-point. As shown by *Figure 7*, a 3-fold increase in the heating rate shifted the maximum only slightly (0.025°C), and the intensity of the scattering lagged behind the positions of the critical scattering pulses, possibly a manifestation of a little hysteresis. The slight increase of the intensities during the slow heating run (▩) above the critical scattering curve is not explained, but probably represents experimental error. Drifts due to variations in laser intensity are mostly, though perhaps not totally, compensated by the base line shift between the beginning and end of the heating run. The extent of this shift is shown at A. The smoothness of the heating runs (▩ and □) shows that short-term intensity stability is excellent, and temperature stability 0.001°C or a little better.

The total time taken for the cloud-point measurements, comprising the cooling run to obtain pulses, and the formation and re-heating of the emulsion, is about 30 minutes.

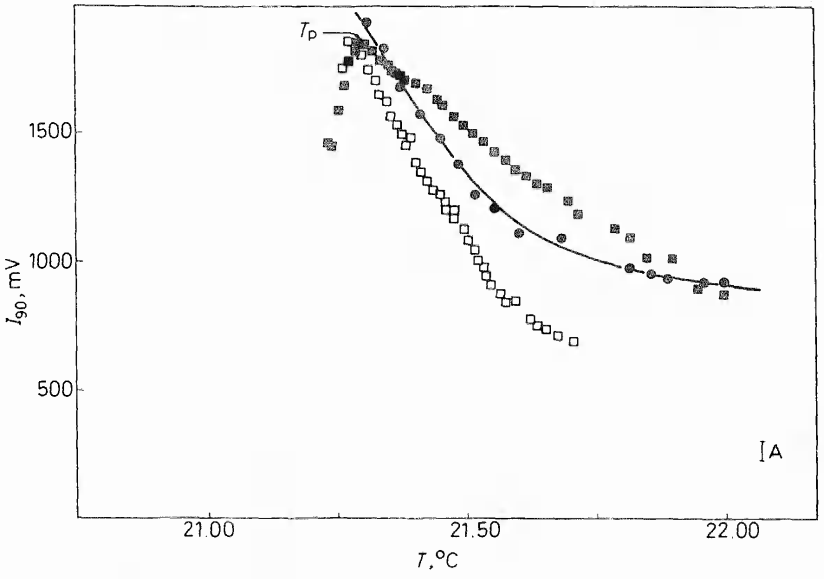

Figure 7. Locating cloud point T_p by the maximum method at high concentration, using a plot of I_{90} vs. T. Solution of 0.084 w/w PS 111, ▩ slow heating rate; □ heating rate 3 times greater. ● Fluctuation scattering intensity I_{90} by pulsed cooling run

6.2 Dilute solutions

In dilute solutions, especially at low molecular weights, I_{90} is weak but I_{30} is very strong (*Figure 4*), and the procedure just outlined for concentrated solutions can be carried out, *mutatis mutandis*, with I_{30}. The first pulse to show evidence of emulsion formation—now by a sudden increase in I_{30} rather than a decline in I_{90}—indicates a suitable temperature T_e for forming the emulsion. The solution is rapidly stepped to T_e and held for about a minute to form the emulsion and to obtain a strong enough I_{30}. Switching on the heating rate of ~ 0.2°C min^{-1} (*Figure 8*) now leads to a rapid decline in I_{30}. The cloud-point T_p is determined to somewhat better than 0.1°C as the point where I_{30} returns to the base line. This base line does not measurably decrease on further heating, i.e. the diminution of fluctuation scattering with temperature is not detected at this great distance from T_s. *Figure 8* also shows that T_p so found is independent of the degree of supercooling over the range of 0.7 to 1.1°C employed. The four plots superpose within experimental error (cf. section 7.2). They fit a curve of type

$$I_{30} = a(T_p - T) + b(T_p - T)^2 \qquad (2)$$

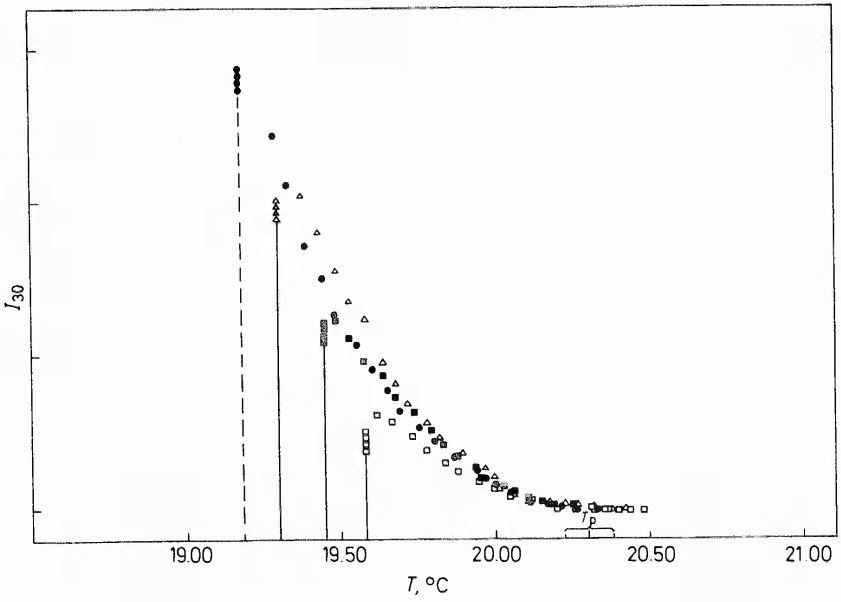

Figure 8. Location of cloud point T_p in dilute solution (0.014 w/w PS 111). Note superposability of four curves especially near T_p, obtained from different degrees of supercooling. ● 19.18; △19.30; ▩19.45; □19.58°C

derived from the simplest theory. The theory makes I_{30} proportional to the volume of a droplet, which varies $\propto (T_p - T)$, and additionally proportional to the polymer concentration in a droplet, which varies linearly with temperature over the small range below T_p concerned.

6.3 Kinetics of phase separation

In dilute solutions of PS–CH, the speed of phase separation can be measured over a range of supercooling, and the results rationalized on simple assumptions. The appropriate model corresponds to the first term in an expansion of the exponential in the well-known Avrami equation for the growth of spherulites. Assuming heterogeneous nucleation, and the usual linear growth rate, the amount of spherulitic material separated initially varies as the third power of time, though later the rate is reduced by impingement of the spheres. In the separation of droplets, the same laws can be applied initially—again the rate will later decline, here because of the change in composition of the continuous phase. Impingements leading to coagulation seems to be negligible over the ranges of supercooling and observation times here employed. The intensity I_{30} should, for sufficiently small drops, vary as the volume of the droplets, so that the initial rate law would be

$$I_{30} = kt^3 \tag{3}$$

The four experimental curves plotted in *Figure 9* do approximately conform

to equation 3, shown as a solid line. All four experimental lines go through the origin and show a prolonged 'induction time'. They have been superposed by scaling the time axis with a deduction of 10 s at the beginning of

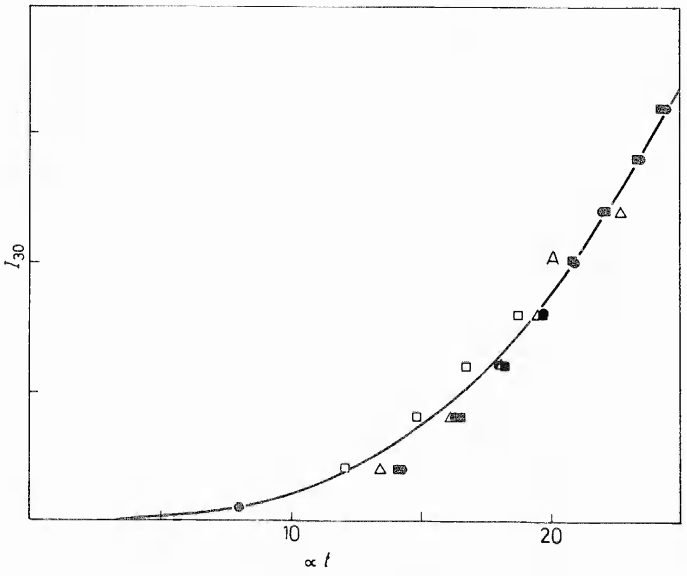

Figure 9. Initial part of plot of intensity I_{30} vs. time in dilute solution (0.014 w/w PS 111). Four runs obtained after sudden stepdown to four different temperatures: ▩18.99; ●19.23; ▲19.51; □19.77°C. The curve drawn is the cubic growth law (equation 3). Time axis scaled for each run to bring point A on the curve; time scale in seconds correct for ●

each run for temperature equilibration. The long thermal equilibration time—about 10 times the response time—arises from the great sensitivity to temperature of the rate of phase separation. The appropriate values of k (equation 3) cover a more than 100-fold range. Two typical pulses (*Figure 10A* and *B*) show the 'induction period', the subsequent initial rise in I_{30} which conforms roughly to equation 3, and the levelling off as the phase change approaches completion. The maximum in I_{90} during the rise in I_{30} confirms the interpretation in terms of growth of spherical objects, since such a maximum is expected as the diameter of the sphere approaches the wavelength of the light (~ 600 nm).

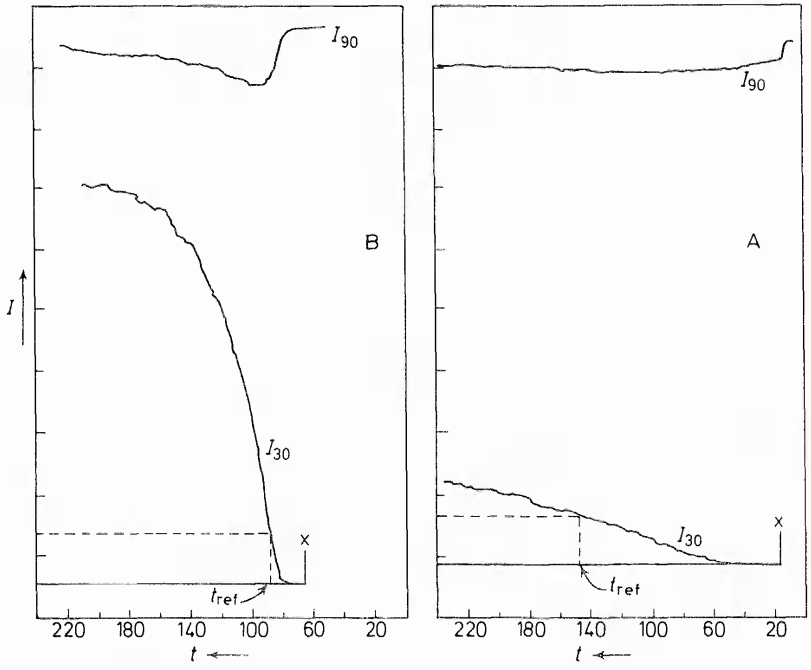

Figure 10. Extended plot of intensity I_{30} (lower curves) and I_{90} (upper curves, inverted) at two different supercoolings on 0.014 w/w PS 111 (cf. *Figure 9*). A 19.58; B 19.18°C. Note the large temperature effect on rate of formation of emulsion. The reference time t_{ref}, taken at an arbitrary low intensity I_{30}, is proportional to the scaling factor in *Figure 9*; its logarithm is plotted as a measure of rate in *Figure 12*

7 DISCUSSION

7.1 Spinodal measurements

Before comparing our results with those of Scholte[6], their relation to the fundamental work of Fisher, Chu[7,8] and their co-workers requires comment. These workers argue that, on the basis of the nature of the mathematical singularities involved at T_c and T_s and on experimental grounds, the classical theory of equation 1 of Debye and co-workers needs to be generalized, essentially to

$$I^{-1} \propto (T - T_s)^{\gamma} \tag{4}$$

This equation is still empirical: γ is no longer unity, but a value of 1.25 may well have universal significance. Their equipment, a purpose-built laser self-beating spectrometer, with excellent temperature control, is suitable for investigating such fundamental points of theory. However, for merely locating T_s, at a concentration not too far from ϕ_c, by extrapolation, it is readily shown that no practical gain is derived from the more elaborate treatment of experimental data. The scattering attenuation correction described by Chu *et al.*[8] has no effect on the apparent T_s, and the volume

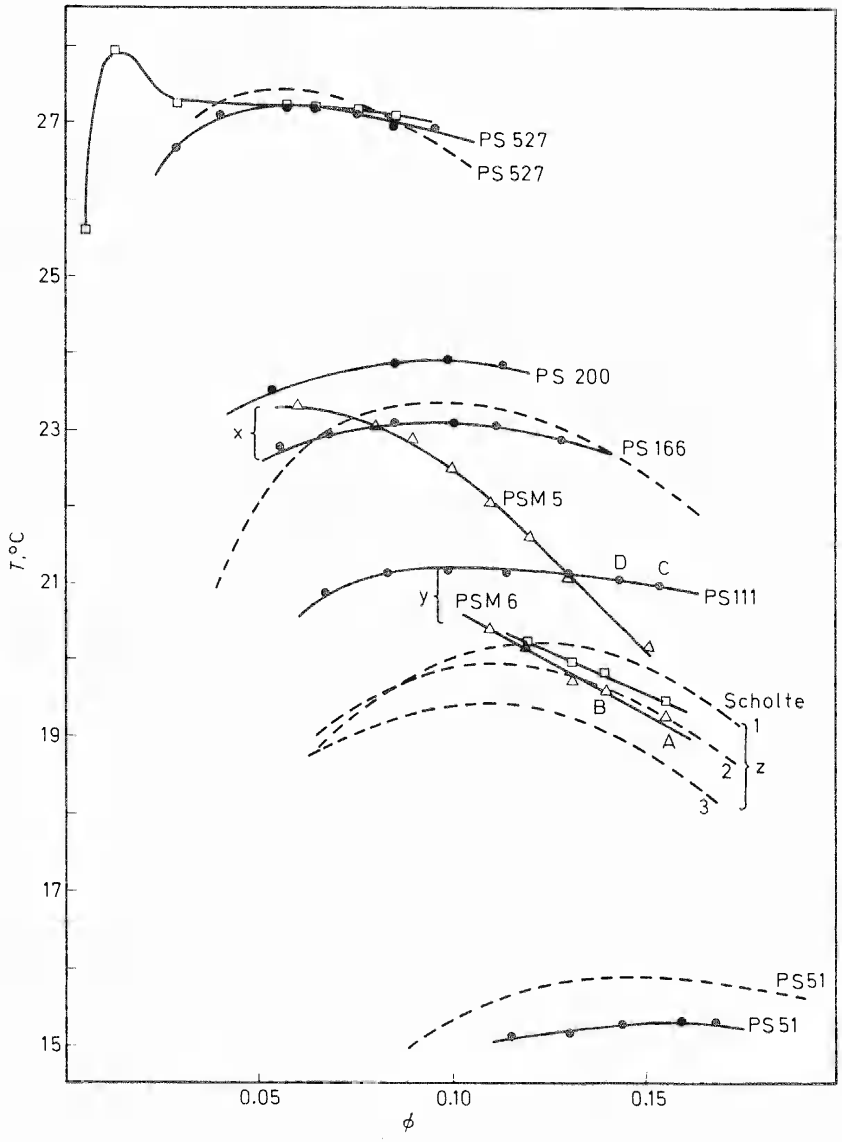

Figure 11. Phase diagram for polystyrene in cyclohexane. – – – – Smoothed data by Scholte[6,11], using conventional light scattering equipment. ——— present data by PICS. Circles: spinodal points; Squares: cloud points. Points A, B, C and D correspond to the points so labelled in *Figure 4*. The braces X, Y, Z link runs at fixed M_w but different M_z. Comparison of the five mixtures PSM 5, PSM 6, and Scholte 1, 2, 3 with their molecular weight averages (*Table I*) suggests that the skew displacement downward of progressively more heterodisperse mixtures correlates with M_z rather than with M_n. Scholte's results on PS 51, PS 166 and PS 527 lie above the PICS results by a few tenths of a degree almost everywhere. Note that a tenfold range in M_w covers a range of about 12 degrees. The Θ-point, corresponding to $M_w = \infty$, lies some 4 to 6°C above the upper limit of the diagram

correction for measurements at different angles has at most a minute effect. Finally, a constant value is subtracted by these authors from each intensity measured on a given solution, in respect of scattering from density fluctuations. Such a correction is included in our term c (Section 5). We adjust this empirically (*Figure 4*) to linearize the classical plot according to equation 1. Chu *et al.* estimate the correction by an arbitrary extrapolation of the scattering intensity to $T_p + 25$. The curved plot in their *Figure 4*, on a solution of PS–CH with $T_p = 26.98$, can be linearized within experimental error by arbitrarily adjusting c downwards ($c < 0$). This procedure merely changes the intercept T_s from 26.4_8 to about 26.5_6°C. As such a small change is hardly significant for our purpose, our base-line correction c is quite justified over the range of concentrations studied. Its effect near ϕ_c is, of course, quite negligible, because the extrapolation is then very short.

The high quality of measurements possible with the equipment of Chu *et al.* is based on a scattering cell of 8 mm diameter, compared with 1 mm for PICS. Accordingly, the thermal response time must be larger by a factor of $\sim 8^2$, i.e. a minute instead of a second. As judged by the smoothness of the plots, and the number and ranges of experimental points included, the data of Chu *et al.* are indeed excellent. It is therefore worrying that the results in their *Figure 1* on PS of $M_w = 4.15 \times 10^5$ in CH, are not in agreement with the approximately concordant results of Scholte and of the present work. Thus their $T_c = 26.95_7$ for PS of $M_w = 4.98 \times 10^5$ is approximately located upon our spinodal for PS of $M_w = 5{\cdot}27 \times 10^5$. This discrepancy is quite unconnected with differences in extrapolating data, and will need further investigation.

Turning to the comparison between Scholte's results and ours, they generally agree to a few tenths of a degree C (*Figure 11*), the precision claimed by Scholte. He used standard light-scattering equipment with a modified temperature control system. He generally collected six intensity measurements on a given solution, covering a 5- to 10-fold range of intensities over a 30 degree C range in temperature. In a later[11] paper, 8 points were spaced at 1°C intervals. In contrast, PICS collects a large number of points closer to T_s, covering (in a few minutes) about a 1 degree C range in temperature, but a similar or larger range of relative intensities (*Figure 5*). Accordingly, PICS gives about 10 times greater precision to the extrapolated value to T_s, and pushes the lower limit of experimentally attainable temperatures as close to T_s as possible, normally a little below the cloud point. With a stiffer polymer than PS, much closer approach to T_s would be possible, as illustrated by the work of Van Aartsen, Smolders and co-workers[12] on the spinodal of solutions of polyoxyphenylene.

7.2 Cloud-point measurements

Nucleation would be expected to control the rate of droplet formation in dilute polymer solutions. Comparison of *Figures 10A* and *B* confirms this, since no other cause is likely for such a large temperature effect implying a negative activation energy. As a result the standard practice of obtaining cloud-points of dilute solutions by cooling clear solutions leads to substantial errors, not eliminated merely by reducing the speed of cooling ever further. The situation is similar to the nucleation of spherulites in bulk polymers

just below T_m. No method exists for studying that equilibrium on any reasonable time-scale, by approaching it from either side. Therefore, a rather long extrapolation, based on nucleation and growth rate theory, is one method for locating T_m. The present work confirms experimentally that phase equilibrium in dilute polymer solution is readily approached from the two-phase (emulsion) side. A simple calculation shows why this would be so. The diffusion of a substrate out of a sphere of radius r into a medium containing a lower constant concentration of that substrate, will be more than 96% complete at the centre of the sphere in r^2/D seconds[13]. The diffusion constant of PS 111 in a dilute solution in CH should be $<5 \times 10^{-7}$ $cm^2\ s^{-1}$. Therefore, equilibrium is practically attained in <1 s for droplets of diameter 10^{-3} cm. Judging by the position of the maximum in I_{90} in *Figure 10A*, our droplets are of diameter approximately equal to the wavelength, say 5×10^{-5} cm, about the time t_{ref} which we use as a measure of their growth rate constant (*Figures 10A* and *B*). They would not grow to a diameter of 10^{-3} cm within the range of the experiments reported. The achievement of equilibrium is strongly supported by the superposability of $I_{30}(T)$ for experiments at different degrees of supercooling (*Figure 8*).

The comparison with nucleation-controlled bulk crystallization may be sketched as follows. Mandelkern[14] found that the rates of crystallization of three polymers, polydecamethylene adipate, polyethylene oxide, and poly-*N*,*N*′-sebacoylpiperazine, respectively passed into the measurable range 5.5, 6, and 12°C below their T_m, and increased by a factor of 10^{12} by further supercooling through respectively 5, 7 and 13°C. In comparison, our rate of droplet growth was measurable *ca.* 0.7°C below T_p and increased by a factor 10^2 over about a further 0.4°C. The absolute rate of droplet formation at fixed $T_p - T$ is much faster than that of spherulite formation at the same $T_m - T$. This reflects the faster transport of chains through the interface in solution, when compared to the bulk. The temperature dependence of the process is much higher for droplets than for spherulites, which reflects the smaller latent heat, and probably also the larger specific surface free energy, accompanying the formation of solution droplets.

The plot in *Figure 12* of the logarithm of the overall rate constant of droplet growth against T has the same kind and degree of curvature as Mandelkern's[14] corresponding plots for the three crystallization systems. He discusses the linearization of the plots by the traditional adjustment upwards (here about 3°C) of the assigned T_m. Our plot in *Figure 12* would require a similar increase in T_p to achieve linearity. Since we contend that the equilibrium point T_p is measurable to about 0.08°C (*Figure 8*), this linearization is not open to the interpretation of phase separation below T_p in solution. However, the curvature may be explained, e.g. because the specific surface free energy of the droplets would increase on cooling, as a result of increasing difference in concentration between the two phases.

Koningsveld and Staverman[15] noted a hysteresis of 0.6°C in apparent T_p on cooling a 1 per cent solution of polyethylene in diphenyl ether, compared to the result on heating the cloudy emulsion. As their turbidimetric measurements were aimed at an accuracy of a few tenths of a degree, this was not considered serious. However, Chu and co-workers aimed at accuracy about 100 times greater, using their purpose-built light scattering photometer for

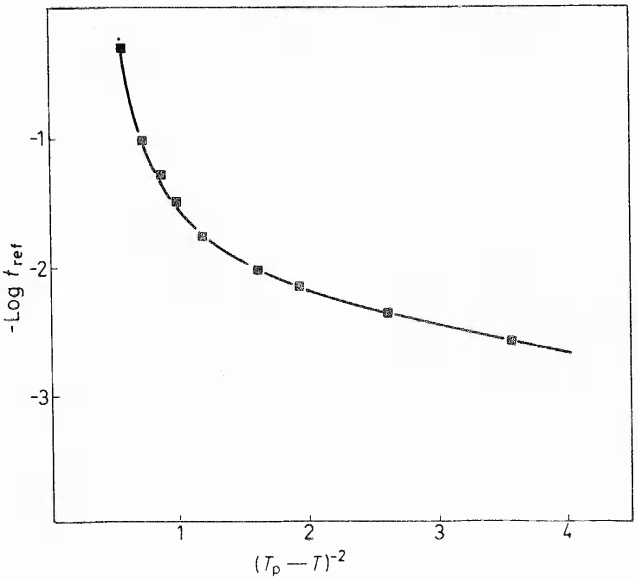

Figure 12. Plot of $-\log t_{ref}$ vs. $1/(T_p - T)^2$ for formation of emulsion from 0.014 w/w PS 111 (cf. *Figure 10*)

measuring T_p by the cooling method only. They reduced the cooling rate to 0.001°C min^{-1}, over ten times slower than that employed by Koningsveld and Staverman. Even so, we believe that their measurement at lowest concentration (~ 0.02 w/w) is likely to be significantly too low because of the expected hysteresis due to nucleation control. Much useful information on transport properties should be obtained by extending our measurements on nucleation and growth kinetics to samples of polymers of different molecular weight, branching, etc.

7.3 The phase diagram

It was realized quite early (see, e.g. Tompa[16]) that the Flory–Huggins (first-approximation) theory—despite its enormous usefulness and its role as a paradigm in polymer science—cannot predict with any accuracy properties which depend on higher derivatives of the free energy of mixing. The spinodal depends on the first Gibbs determinant (cf. Koningsveld[1]) involving second derivatives, and the critical point on the second determinant, which involves third derivatives, with respect to concentration. Even though phase diagrams in general are thus poorly predicted by the crude theory, it can be used to explore, as a heuristic model, for instance, the effects of polydispersity on the cloud point curve (Šolc[17], Koningsveld and Staverman[15]). A great step forward was taken by Koningsveld and his co-workers, when they showed that the interaction parameter χ of the Flory–Huggins model can be turned into an arbitrary function of overall polymer concentration, without unduly complicating the mathematics. From this much

more general second-approximation theory, it was deduced that the spinodal of solutions of linear polymers depends only on M_w, and the critical point only on M_w and M_z. As a third approximation (Ref. 18), even effects of end-groups, branch units and copolymerization remain tractable within the framework of this theory, but some dependence on M_n is thereby introduced. At least one further factor is certain to require attention before a complete theory of phase diagrams can emerge: the effects introduced when one of the phases in an equilibrium is too dilute to conform to models of the Flory–Huggins type, which require substantial intermingling of polymer coils in solution. This situation is commonly encountered in practice. Fortunately, a promising theory—not costly in terms of adjustable parameters—has just been developed to meet it (Koningsveld, Stockmayer, Kennedy and Kleintjens[19]).

The most obvious application of a phase diagram, such as *Figure 11*, is to the characterization of polymer distributions, especially by reference to M_w and M_z. Despite their relatively high speed, PICS measurements are seen to give results of high accuracy as shown by the relative smoothness of the spinodal loci. The phase diagram suggests that the M_w of a sharp fraction could, after suitable calibration, be measured to 3 per cent at $M_w = 5 \times 10^5$ and to 1 per cent at 5×10^4. As this is somewhat better than the primary calibration of the M_w of the fractions, PICS measurements would be suitable for smoothing primary calibrations.

The two curves PSM5 and PSM6 show that the spinodal of highly heterodisperse samples deviate strongly from that of a sharp fraction of equal M_w (respectively PS 111 and PS 166), contrary to the result of the second-approximation theory. The same effect was observed by Scholte[11], who thought that this might be taken into account by a term depending on M_n in the free enthalpy of mixing (cf. the end-group effect[18]). However, comparing Scholte's results with ours (*Figure 11* and *Table 1*), it is clear that the deviation of the spinodal of a heterodisperse mixture from that for the sharp fraction of the same M_w, is governed much more exactly by M_z/M_w than by M_w/M_n. The deviations from the second-approximation theory exposed by *Figure 11*, do not invalidate the principle of characterizing polymer distributions by T_s and T_c. Clearly, the measurements are even *more* sensitive to the molecular weight averages than previously thought, and at worst this calls for more extensive calibration procedures, which are not time-consuming with PICS.

The spike at low concentration on the T_p curve of PS527 is interesting. It would easily be missed by approaching the equilibrium from the homogeneous side. The technique of heating a carefully 'seeded' emulsion, establishes the existence of the spike beyond doubt (though its detailed course has not been accurately charted). Koningsveld and Staverman found by theoretical calculation that such spikes would result from, and be sensitive to, heterodispersity. PS527 is a reputable sharp but by no means homodisperse (*Table 1*) fraction. The experimental finding of the spike is a further confirmation, not only of the sensitivity of phase equilibrium measurements, but of their successful modelling by theoretical calculations. The combined measurements by Scholte, using conventional light scattering, and ours using PICS, in *Figure 11*, should help in improving the theory of the free enthalpy function beyond the second approximation.

ACKNOWLEDGEMENT

We gratefully acknowledge financial assistance of this work by Applied Research Laboratories Limited, and a studentship for K.W.D. from ICI Plastics Division. We thank Mr B. Ready for designing and building electronic circuits and Mr Gary Stoneham for technical assistance.

REFERENCES

[1] R. Koningsveld, *Disc. Faraday Soc.* **49** (1970); R. Koningsveld and L. A. Kleintjens. *Macromolecular Chemistry 8* (K. Saarela, ed.), p. 197, Butterworths, London (1973).
[2] P. Debye, *J. Chem. Phys.* **31**, 680 (1959).
[3] P. Debye, H. Coll and D. Woermann, *J. Chem. Phys.* **33**, 1746 (1960).
[4] P. Debye, B. Chu and D. Woermann, *J. Chem. Phys.* **36**, 1803 (1962).
[5] A. Vrij and M. W. J. Van den Esker, *J. Chem. Soc., Faraday II* **68**, 513 (1972).
[6] Th. G. Scholte, *J. Polymer Sci., A-2*, **9**, 1553 (1971).
[7] B. Chu, F. J. Schoenes and M. E. Fisher, *Phys. Rev.* **185**, 219 (1969).
[8] N. Kuwahara, D. F. Fenby, M. Tamsky and B. Chu, *J. Chem. Phys.* **55**, 1140 (1971).
[9] J. Goldsbrough, *Sci. Prog., Oxf.* **60**, 281 (1972).
[10] H. A. G. Chermin, M. Gordon and R. Koningsveld, *Macromolecules* **2**, 207 (1969).
[11] Th. G. Scholte, *J. Polymer Sci., C* **39**, 281 (1972).
[12] C. A. Smolders, J. J. van Aartsen and A. Steenbergen, *Kolloid-Z. Z. Polymere* **243**, 14 (1971); P. T. Van Emmerik and C. A. Smolders, *J. Polymer Sci., C* **38**, 73 (1972).
[13] J. Crank, *The Mathematics of Diffusion*, p 86, Clarendon Press, Oxford (1964).
[14] L. Mandelkern, *Chem. Rev.* **56**, 903 (1956).
[15] R. Koningsveld and A. J. Staverman, *J. Polymer Sci., A-2*, **6**, 349 (1968).
[16] H. Tompa, *Polymer Solutions*, p. 208 Butterworths, London (1956).
[17] K. Šolc, *Macromolecules*, **3**, 665 (1971).
[18] J. W. Kennedy, M. Gordon and R. Koningsveld, *J. Polymer Sci. C* **39**, 43 (1972).
[19] R. Koningsveld, W. H. Stockmayer, J. W. Kennedy and L. A. Kleintjens, in press.